Geophysical Journal International

Geophys. J. Int. (2017) **209,** 1408–1417
Advance Access publication 2017 March 9
GJI Gravity, geodesy and tides

doi: 10.1093/gji/ggx099

Cooperating the BDS, GPS, GLONASS and strong-motion observations for real-time deformation monitoring

Rui Tu,[1,2,3] Jinhai Liu,[1,2] Cuixian Lu,[4] Rui Zhang,[1,3] Pengfei Zhang[1,2] and Xiaochun Lu[1,2,3]

[1]*National Time Service Center, Chinese Academy of Sciences, Shu Yuan Road,* 710600 *Xi'An, China. E-mail: turui-2004@126.com*
[2]*University of Chinese Academy of Sciences, Yu Quan Road,* 100049 *Bei'Jing, China*
[3]*Key Laboratory of Precision Navigation and Timing Technology, Chinese Academy of Sciences, Shu Yuan Road,* 710600 *Xi'An, China*
[4]*German Research Center for Geosciences, Telegrafenberg, D-*14473 *Potsdam, Germany*

Accepted 2017 March 8. Received 2017 March 6; in original form 2016 October 7

SUMMARY

An approach of cooperating the BDS, GPS, GLONASS and strong-motion (SM) records for real-time deformation monitoring was presented, which was validated by the experimental data. In this approach, the Global Navigation Satellite System (GNSS) data were processed with the real-time kinematic positioning technology to retrieve the GNSS displacement, and the SM data were calibrated to acquire the raw acceleration; a Kalman filter was then applied to combine the GNSS displacement and the SM acceleration to obtain the integrated displacement, velocity and acceleration. The validation results show that the advantages of each sensor are completely complementary. For the SM, the baseline shifts are estimated and corrected, and the high-precision velocity and displacement are recovered. While the noise of GNSS can be reduced by using the SM-derived high-resolution acceleration, thus the high-precision and broad-band deformation information can be obtained in real time. The proposed method indicates a promising potential and capability in deformation monitoring of the high-building, dam, bridge and landslide.

Key words: Satellite geodesy; Space geodetic surveys; Transient deformation.

1 INTRODUCTION

Global Positioning System (GPS) and strong motion (SM) are two effective and valuable tools for deformation monitoring. Each of the two sensors shows its advantages and drawbacks. In terms of GPS, both real-time kinematic (RTK) and precise point positioning (PPP) approaches can be used to retrieve the displacement with an accuracy ranging from centimetres to millimetres (Blewitt 1989; Zumberge *et al*. 1997), which can be further improved benefiting from the integer ambiguity resolution (Blewitt 1989; Dong and Bock 1989; Ge *et al*. 2008; Geng *et al*. 2010; Li *et al*. 2011). However, due to the limitation of sample rates, the GPS-derived velocity and acceleration reveal large noises (Genrich & Bock 2006; Elósegui *et al*. 2006). Besides, simultaneous observations from two stations are needed for the RTK positioning (Blewitt 1989), and the high-precision ephemeris products have to be provided in the PPP which also shows a feature of a long initialization time (Cai and Gao 2007; Jokinen *et al*. 2011). Although the recent development on speeding up PPP initialization can rely on the undifferenced ambiguities with multi-Global Navigation Satellite System (GNSS) combination in simultaneous, at least 20 min or even longer time is still required (Geng *et al*. 2011; Geng & Shi 2017; Liu *et al*. 2017). The newly developing velocity estimation technology is more challenge for the real-time deformation monitoring as it can be operated by using the broadcast ephemeris products with a station-alone single-frequency receiver (Colosimo *et al*. 2011; Li *et al*. 2013b,2015c; Tu 2014). But this approach needs to remove the initial shift and is only applicable for monitoring the short-period deformation. In addition, Xu *et al*. (2013) proposed to use the high-rate PPP to measure the seismic wave motions, where the inertial measurement units were utilized as independent comparison and validation.

Concerning the SM, it displays the advantages of high accuracy and high temporal resolution acceleration records (Wang *et al*. 2013; Javelaud *et al*. 2011), which, however, might be biased by the so-called baseline errors that are mainly caused by ground shaking like tilting and/or rotation of the instruments, and might be seriously distorted when integrated into velocity and/or displacement (Iwan *et al*. 1985; Boore 2001; Wu & Wu 2007; Wang *et al*. 2011). Although many empirical baseline correction approaches can be used to correct them, the recovered results still display a large offset and are not applicable in real time (Wang *et al*. 2013).

The complementary advantages of high-rate GPS and accelerometer measurements have been widely recognized and several approaches have been proposed for the integration of the two data sets. These studied can be classified into two categories. The first one is loose

integration, which mainly applies high-precision GPS displacement to correct the baseline shifts and to recover the deformation information. Emore *et al*. (2007) presented combining GPS and seismic data to retrieve optimal near-source displacements. The high-precision GPS displacement was used to constrain the long-period instability during integration of accelerometer records and correct for any unpredictable offsets presented in GPS that may be approximated as step functions. Bock *et al*. (2011) proposed a methodology to optimally estimate the displacement in near real time from a combination of the GPS relative positioning displacements and raw accelerometer acceleration records by a Kalman filter. It may avoid problematic baseline shifts to some extent. However, the baseline shifts are still not easy to be constrained, as they cannot be completely absorbed by the dynamic noises of the filter, resulting in the recovered results of a large offset. In Wang *et al*. (2013), a trigonometric function polynomial was formed to express the baseline shifts, and a least-squares solution was used to determine the baseline shifts by making the corrected displacements optimally consistent with the high-rate GPS displacement. With their approach, the high-precision velocity and displacement can be retrieved to some extent, but the assumptions of the trigonometric function polynomial are affected by subjective factors due to the complicated baseline shifts, and this method cannot be operated in real time. Tu *et al*. (2013) presented a cost-effective approach to retrieve high-precision and broad-band ground motion waves by joint use of a single-frequency GPS and an MEMS accelerometer, which was validated by analysis of an experimental data set.

The second one is tight integration: the raw GPS and acceleration observations are directly combined to obtain high-precision deformation information. In Geng *et al*. (2013a), the baseline shifts are modeled as random walk processes to be estimated together with displacement. The results showed that GPS networks upgraded with SM accelerometers could provide new information for improved understanding of the earthquake rupture process. Li *et al*. (2013a) made use of accelerometers data after applying empirical baseline shifts correction, in order to strengthen GPS solutions for better integer ambiguity-fixing and consequently better accuracy. And Tu *et al*. (2014) also proposed another approach, where the baseline error estimated from a previous epoch was introduced in real time into the state equations at the current epoch. In this approach, the station position related state parameters could be successfully constrained and the baseline errors could be estimated. In addition, Chen *et al*. (2015) proposed the integration of GNSS and Inertial Navigation System (INS) for measuring the irregularity of the railway track.

Up to now, the integration is usually operated by a single GNSS and an SM sensor, the reliability and continuous may not be well guaranteed under some conditions such as during the loss of GNSS data or when a fewer satellites are tracked. In addition, the joint use of multiconstellation and multifrequency observations has become the trend of GNSS development, providing more reliable results (Li *et al*. 2015a,b). Thus, the combination of BeiDou System (BDS), GPS, GLONASS and SM data are of great interest and need further investigation.

Based on these backgrounds mentioned previously, this study presents an integration method of cooperating the BDS, GPS, GLONASS and SM observations for real-time deformation monitoring. First, the integration approach is introduced, and then the experimental data are used for the validation and analysis; finally, some conclusions and discussions are provided.

2 METHODOLOGIES

2.1 Real-time retrieval of high-precision GNSS displacement by RTK

For the RTK solution, we used the double-differenced (DD) model (Yanase *et al*. 2010). The linearized DD pseudo-range and carrier phase observation equations for the BDS, GPS and GLONASS are expressed as following:

$$\begin{cases} P_{br}^{kj,G} = l_r^{kj,G}\Delta X_r + m_r^{kj,G}\Delta Y_r + n_r^{kj,G}\Delta Z_r + I_{br}^{kj,G} + T_{br}^{kj,G} + \rho_{br}^{kj,G} + \varepsilon_P^G \\ P_{br}^{kj,R} = l_r^{kj,R}\Delta X_r + m_r^{kj,R}\Delta Y_r + n_r^{kj,R}\Delta Z_r + I_{br}^{kj,R} + T_{br}^{kj,R} + \rho_{br}^{kj,R} + \varepsilon_P^R \\ P_{br}^{kj,C} = l_r^{kj,C}\Delta X_r + m_r^{kj,C}\Delta Y_r + n_r^{kj,C}\Delta Z_r + I_{br}^{kj,C} + T_{br}^{kj,C} + \rho_{br}^{kj,C} + \varepsilon_P^C \\ \lambda^G\phi_{br}^{kj,G} = l_r^{kj,G}\Delta X_r + m_r^{kj,G}\Delta Y_r + n_r^{kj,G}\Delta Z_r - I_{br}^{kj,G} + T_{br}^{kj,G} + \rho_{br}^{kj,G} - \lambda^G \mathrm{Amb}_{br}^{kj,G} + \varepsilon_\phi^G \\ \lambda^{j,R}\phi_{br}^{j,R} - \lambda^{k,R}\phi_{br}^{k,R} = l_r^{kj,R}\Delta X_r + m_r^{kj,R}\Delta Y_r + n_r^{kj,R}\Delta Z_r - I_{br}^{kj,R} + T_{br}^{kj,R} + \rho_{br}^{kj,R} \\ \qquad\qquad - \lambda^{j,R}\mathrm{Amb}_{br}^{kj,R} + (\lambda^{j,R} - \lambda^{k,R})\mathrm{Amb}_{br}^{k,R} + \varepsilon_\phi^R \\ \lambda^C\phi_{br}^{kj,C} = l_r^{kj,C}\Delta X_r + m_r^{kj,C}\Delta Y_r + n_r^{kj,C}\Delta Z_r - I_{br}^{kj,C} + T_{br}^{kj,C} + \rho_{br}^{kj,C} - \lambda^C \mathrm{Amb}_{br}^{kj,C} + \varepsilon_\phi^C \end{cases} \quad (1)$$

where P, Φ are the pseudo-range and carrier phase observables, respectively, the subscripts b and r represent the base and user receivers, respectively and the superscripts k and j represent the pair of satellites with k being the reference one. Subscripts G, R and C denote the GPS, GLONASS and BDS system, respectively. $(\cdot)_{br}^{j}$ and $(\cdot)_{br}^{k}$ express the single difference between stations, $(\cdot)_{br}^{kj}$ is the DD between stations and satellites. The symbols l, m and n are the unit vectors along the line of sight from receiver to satellite. The baseline components ΔX, ΔY, and ΔZ are to be solved, Amb is the integer ambiguity of the carrier phase and I and T are the ionospheric delay and tropospheric delay, respectively. ε is the measurement noise, its standard deviation is δ, and ρ is the geometric distance from satellite to receiver.

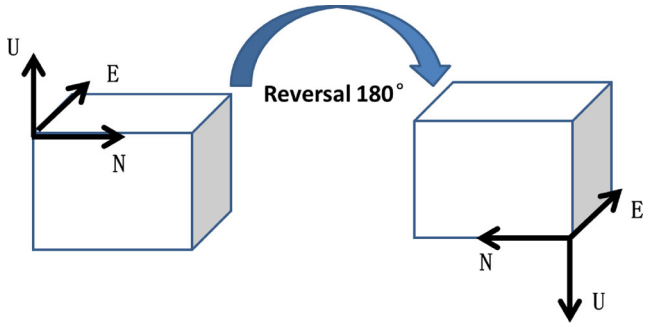

Figure 1. The calibration of the strong-motion sensor.

The weight matrix is written as eq. (2), it is determined by the observation noise. The phase noise is 0.002 m, and the noise ratio between pseudo-range and the phase is setup as 100, the weight among different systems is treated as equal weight.

$$P = \begin{bmatrix} 1/[\delta_P^G]^2 & & & & & & \\ & 1/[\delta_P^R]^2 & & & & & \\ & & 1/[\delta_P^C]^2 & & & & \\ & & & 1/[\delta_l^G]^2 & & & \\ & & & & 1/[\delta_l^R]^2 & & \\ & & & & & 1/[\delta_l^C]^2 & \end{bmatrix}. \tag{2}$$

For the RTK solution, where the distance between the reference and rover stations is very short (a few kilometres), the DD ionospheric and tropospheric residuals can be ignored. The estimated parameters are the baseline components and the ambiguities. For the parameters estimation, the baseline components is estimated at each epoch, and the DD phase ambiguity is estimated as a constant for each continuous period which should be reinitialization when a cycle slip is occurred. Generally, the float ambiguities need a short time to complete the initialization, so we use the lambda approach for the ambiguities resolution to speed up the solution convergence.

2.2 Real-time retrieval of high-resolution acceleration by instrument calibration

SM sensor is a type of acceleration survey equipment. The accelerometer can measure precisely up to a few millimetres and has a general sampling rate at 80–200 Hz. Usually, for the digital storage and record reasons, the outputs of the SM is integer counts instead of the acceleration. Thus, in order to transfer the integer counts into raw acceleration, all the SM sensors need to carry out the instrument calibration (Fleming *et al*. 2009).

The instrument calibration can be performed following the description illustrated in Fig. 1. Taking the vertical component as an example, first, take the instrument in the horizontal position and keep the vertical component upwards, record the data for several minutes, then reversal 180° to keep the vertical component down, and record the data for another several minutes. The counts difference between the two times is twice of the acceleration, thus the instrument calibration parameter in the vertical component can be recovered, as shown in eq. (3). Similar method can be applied for the other two components to be calibrated

$$a = \Delta\text{counts}/2. \tag{3}$$

2.3 Real-time integration estimation by the cooperation of GNSS and SM records

For the integration estimation of the cooperated GNSS and SM records, a Kalman filter model can be used. The inputs are the GNSS displacements and the SM acceleration, and the outputs are the combined displacements, velocity, acceleration and SM's baseline shifts.

As the baseline shifts can happen at any time and vary temporarily, especially during the motion period when the variation of the station state is rather swift, defining the optimal dynamic state noises are of importance for the integration results. The dynamic state noises not only describe the state variations but also contain the biases induced by the baseline errors. As the biases are much difficult to be precisely determined, the filtered solution is usually affiliated with a large offset. To overcome these drawbacks, we improve the method by adding the baseline shifts as unknown parameters and estimate them as random-walk processes. The observation and state equations can be updated as following (Tu *et al*. 2014),

$$[s]_k = \begin{bmatrix} 1 & 0 & 0 \end{bmatrix}_k \begin{bmatrix} d \\ v \\ u \end{bmatrix}_k + [\alpha]_k[\alpha]_k \sim N\left(0, R^S\right) \tag{4}$$

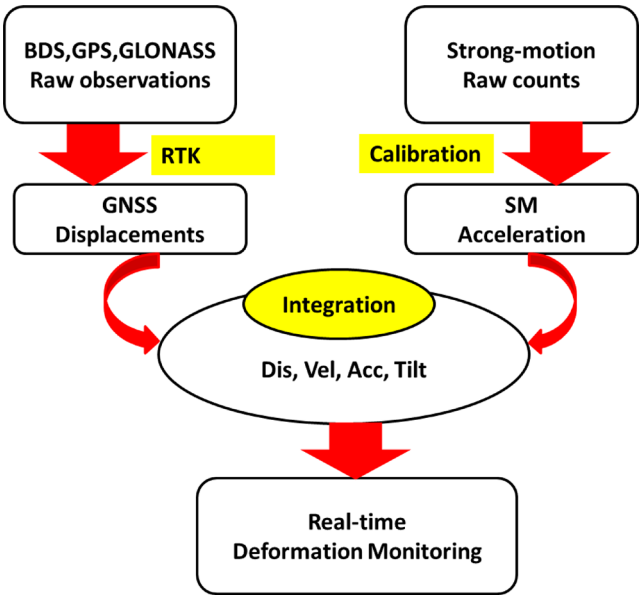

Figure 2. The data processing flow.

$$\begin{bmatrix} d \\ v \\ u \end{bmatrix}_k = \begin{bmatrix} 1 & t_a & -0.5t_a^2 \\ 0 & 1 & -t_a \\ 0 & 0 & 1 \end{bmatrix}_k \begin{bmatrix} d \\ v \\ u \end{bmatrix}_{k-1} + \begin{bmatrix} 0.5t_a^2 \\ t_a \\ 1 \end{bmatrix} [a]_k + [\beta]_k [\beta]_k \sim N\left(0, Q^S\right) \tag{5}$$

$$\left[R^S\right] = \left[\frac{r}{t_d}\right] \left[Q^S\right] = \begin{bmatrix} qt_a^5/20 & qt_a^4/8 & qt_a^3/6 \\ qt_a^4/8 & qt_a^3/3 & qt_a^2/2 \\ qt_a^3/6 & qt_a^2/2 & qt_a^1/1 \end{bmatrix} \tag{6}$$

where s and a are the GNSS displacement and accelerometer acceleration, respectively, d and v denote the combined displacement and velocity, respectively. t_a and t_d describe the sampling intervals of the accelerometer and GNSS, respectively, k is the epoch number. R^S and Q^S represent the observation noises and dynamic state noises. q is the acceleration variance and r is the GNSS measurement noise variance. u is the baseline shift. Attributing to these improvements, the baseline shifts problems are solved and the corrected high-resolution acceleration can also provide accurate state information for the integration solution. With eqs (4)–(6), the combined solution can be easily obtained by means of a Kalman filter (Bock *et al*. 2011).

2.4 The realization process

The realization of cooperating the BDS, GPS, GLONASS and SM observations for real-time deformation monitoring can be summarized in Fig. 2.

First, collocate the BDS, GPS and GLONASS raw observations and perform the RTK solution to get the GNSS displacement; simultaneously, the SM's raw counts are transferred into raw acceleration. To be noted, the instrument calibration should be carried out before the installing.

Second, the GNSS displacements and the SM acceleration are integrated to obtain the combined displacement, velocity, acceleration and baseline shift, in order to be applied for the real-time deformation monitoring.

3 VALIDATION AND ANALYSIS

3.1 Experiment introduction

Fig. 3 shows the platform that we used in the experiment carried out in 2016 August in Xi'An, China. The platform, which can slide along a table, includes a dynamic GNSS antenna that can track the BDS, GPS and GLONASS signals (Type: UR380, Antenna: HX-GG486A), and a low-cost MEMS-type accelerometer (Fleming *et al*. 2009). The sampling rate is 1 Hz for the GNSS and 100 Hz for the accelerometer. The maximum sliding distance of the platform is restricted to about 0.5 m. All the data are processed in a simulated real-time mode. We simulated eight experiments by moving the platform from one side to the other. The reference displacements are recorded by the vernier caliper which is

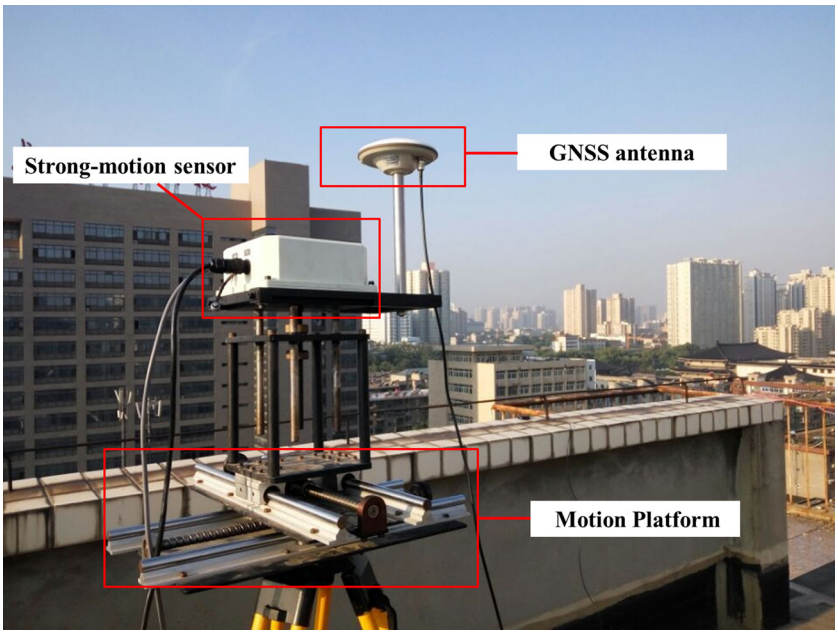

Figure 3. Experimental set up, consisting of a GNSS receiver, a strong-motion sensor and a sliding platform.

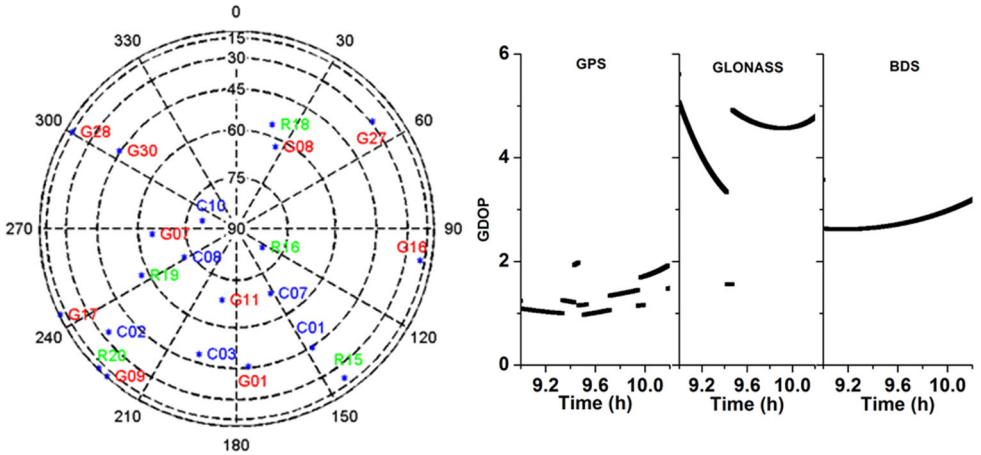

Figure 4. The satellite geometry (left-hand side) and the GDOP values (right-hand side). (The GPS satellites are shown in red, the GLONASS satellites in green and the BDS satellites in blue.)

fixed on the table. For each experiment, we kept the rig static at the start point for about several minutes at first; second, we slid the combined instruments from the start point to the endpoint over about one or two minutes; third, the rig was kept static at the endpoint for about several minutes, before starting the next experiment. To sum up, we carried out eight experiments in the horizontal component, three times in the south–north direction, three times in the east–west direction and two times in the direction from west-south to east-north.

3.2 Results analysis

Fig. 4 shows the satellite geometry and the geometric dilution of precision (GDOP) values. During the experiment, the averaged number of satellites in view is 6, 10 and 5 for BDS, GPS and GLONASS, respectively. In terms of the GDOP, GPS shows smaller value than BDS and GLONASS. Besides, GLONASS displays the largest GDOP values, which indicates that the precision derived from GLONASS is the worst.

Fig. 5 shows the raw GNSS displacement and SM acceleration. It can be found that the precision of GLONASS system is the worst as the observed satellites is less, especially in the vertical component. The BDS and GPS system nearly show the same accuracy. And for the raw acceleration, it reveals some baseline shift errors as the acceleration is not zero at the end of the experiment, which will be discussed further in the following section.

Fig. 6 shows the results of the first experiment. Although the velocity and acceleration obtained from the GNSS-only solution are very noisy, the displacement reflects the reality with an uncertainty of a few millimetres. In comparison, the SM-based acceleration has a much higher signal-to-noise ratio, but the baseline shift corrected velocity and displacement show a larger offset than those of GNSS. Here, the

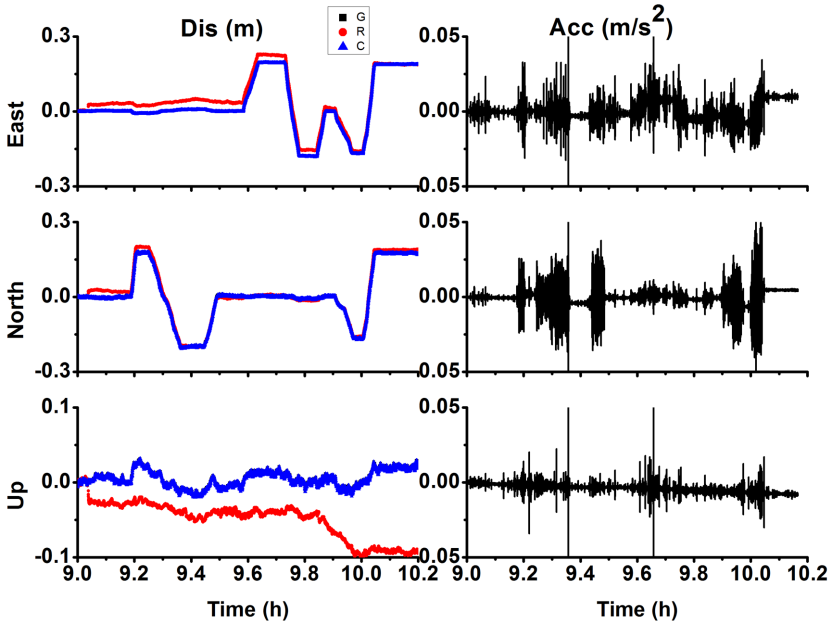

Figure 5. The raw GNSS displacement (left-hand side) and the SM acceleration (right-hand side) ('G', 'R' and 'C' represent GPS, GLONASS and BDS, respectively, here the GPS and BDS displacements display nearly the same pattern, thus the black and blue lines are overlapped).

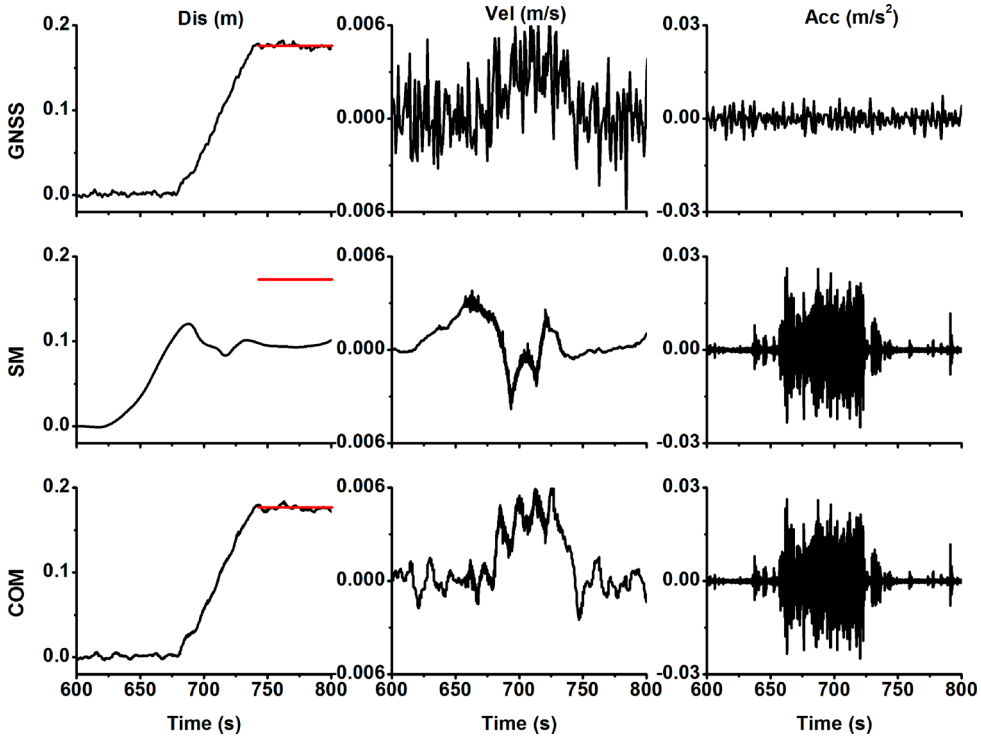

Figure 6. The example of the first experiment. From top to bottom are the results retrieved from GNSS, SM and the combined system (COM); from left to right are the time-series of displacement, velocity and acceleration, respectively. The red line describes the final reference displacement.

baseline shift correction is derived using the empirical approach proposed by Wang *et al*. (2013). While for the combination of GNSS and SM measurements, not only are the velocity and displacement recovered, but also the displacement reveal much smaller noise.

In addition, Fig. 7 shows the power spectral densities of the displacements by different observations. It can be clearly seen that the combined system complements the advantages of the two techniques.

In Fig. 8, the results of cooperating the BDS, GPS and GLONASS data for all the eight experiments are illustrated. As expected, when the baseline shifts of the accelerations are corrected by the combined system, the high-resolution acceleration can help to constrain the combination solution. Thus, the high-precision and broad-band deformation information (displacement, velocity and acceleration) in real

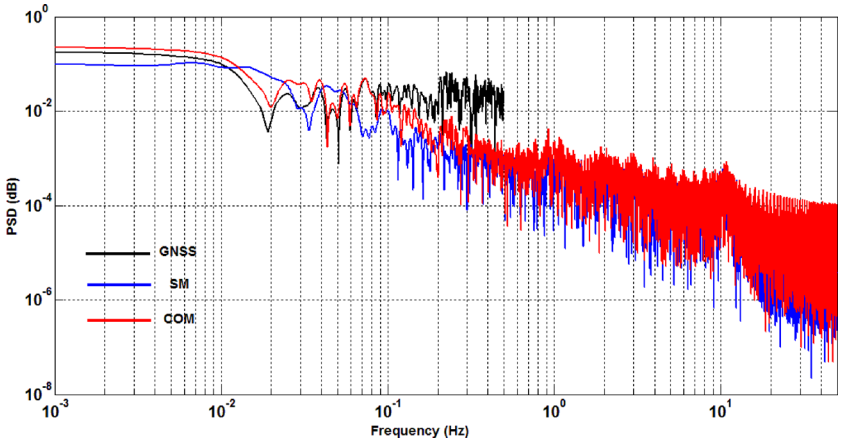

Figure 7. The comparison of the PSD for the displacements of the first experiment by different observations. (The black, blue and red lines represent the GNSS, SM and the combined system, respectively.)

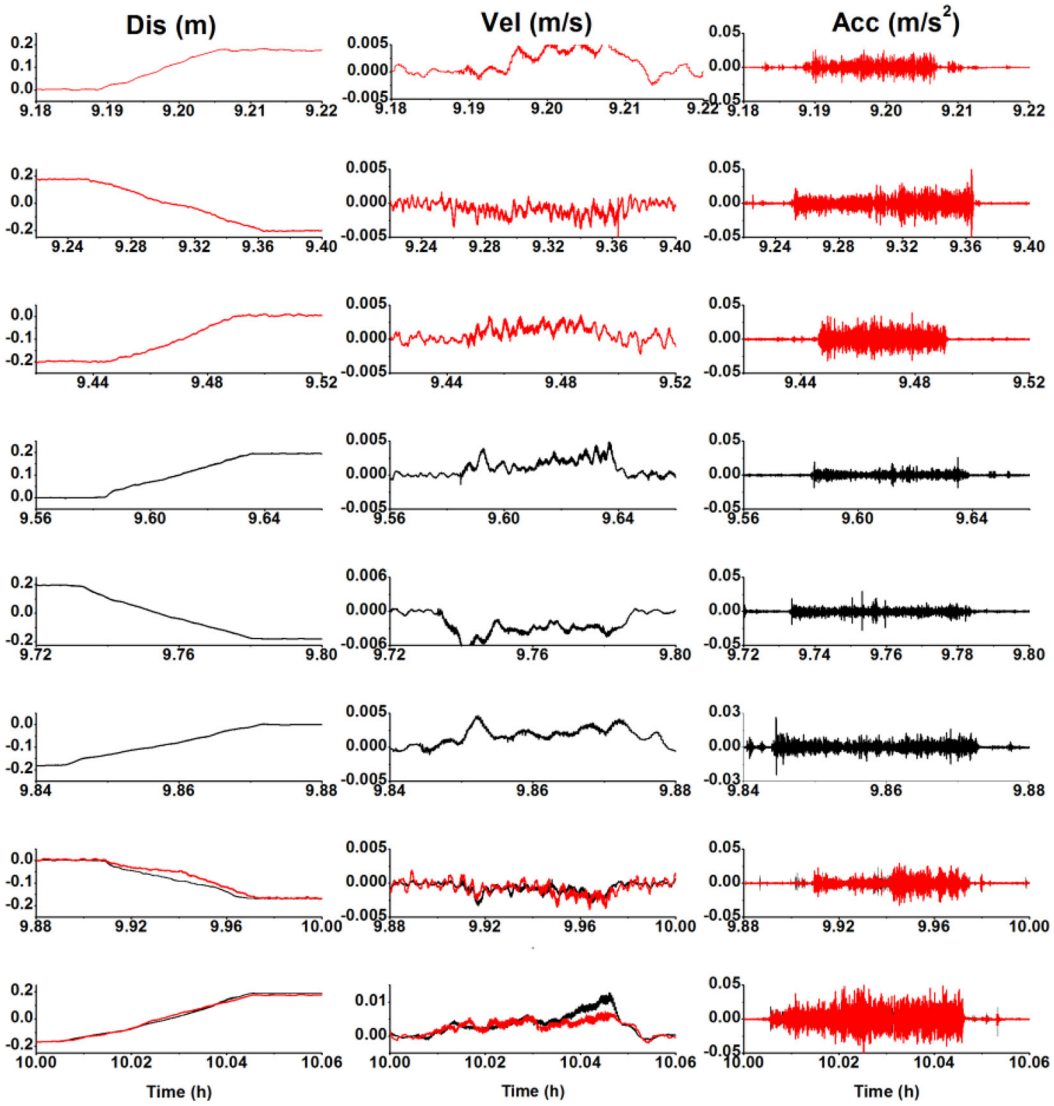

Figure 8. Results of all the eight experiments. From left to right are the time-series of combined displacement, velocity and acceleration, respectively. From top to bottom are the experiments from one to eight, respectively. (The red line marks the north component and black line marks the east component.)

Table 1. Rms deviations between the recovered values and reference displacements (unit: centimetres).

Experimental number	Rms east (cm)	Rms north (cm)
1	/	0.40
2	/	0.32
3	/	0.35
4	0.36	/
5	0.42	/
6	0.35	/
7	0.38	0.32
8	0.34	0.37

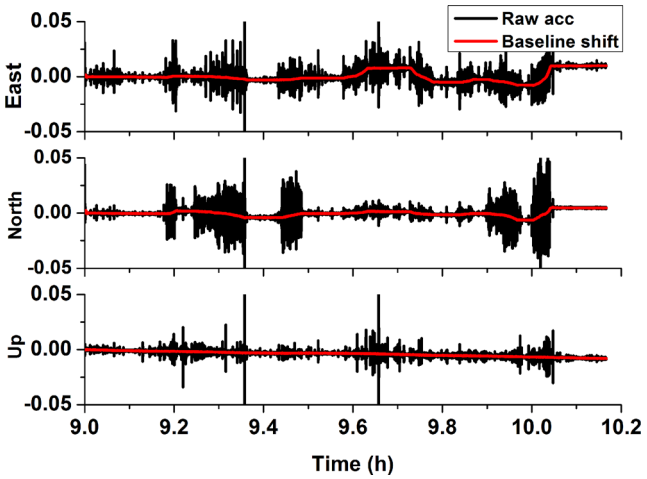

Figure 9. The time-series of the estimated baseline shift error (from top to bottom are the east, north and vertical components, respectively).

time are recovered. Table 1 summarizes the root mean square (rms) deviations between the recovered values and reference displacements. One can note that the rms is generally less than 5 mm.

As for the combination of the BDS, GPS, GLONASS and SM measurements, the key issue is the precise processing of the SM's baseline shift error. For the empirical methods, the baseline shift correction of the acceleration is divided into three parts, the pre-event, the transient part and the post-event according to the characteristics of the acceleration. Meanwhile, the integrated velocity is corrected with a continuous double broken line (Wang *et al*. 2011). This means that the baseline shifts of the acceleration are treated as a constant in the motion period. As shown in Fig. 9, the baseline shift is changing, as the tilting and/or rotation of the instrument is not a simple event when the ground is shaking during the whole motion period. Due to the variation of the baseline shifts all the time, these empirical methods are not objective and have large uncertainties. In this study, the baseline shifts of the acceleration are estimated and corrected as continuous unknown parameters. It is less subjective and more accurate to describe the baseline shifts, so the optimal displacement, velocity and acceleration information can be retrieved from the combined system.

Moreover, the baseline shift error is not only the product of translation and rotation of ground, but also the information of ground tilting during the motion period. By combining the collocated GNSS and SM records, we can both estimate the baseline shift, and recover the coseismic point ground tilting (Geng *et al*. 2013b). Fig. 10 shows the correlation between the baseline shift error and ground tilting. As shown in the experiment results, there is a strong linear correlation between the baseline shift error and ground tilting, representing by the red linear fitting curve in Fig. 10. The coefficients and accuracy of the linear equation are also displayed. One can see that the intercept of curve on the vertical axis is very small, nearly equal to zero. Thus, a strong direct proportional relationship exists between the baseline shift error, so does the ground tilting, that is, baseline shift error (y) = proportion coefficient (b) * tilting angle (x) + a. Meanwhile, according to the proportion coefficient 'b', a proportion coefficient of about 10 can be found, which can be regarded as the gravitational acceleration constants. Therefore, one can conclude that the baseline shift error is mainly the projection of gravitational acceleration on the tilting angle component, and the baseline shift error caused by environmental noises is far less than those induced by the ground tilting and rotation.

4 CONCLUSIONS AND DISCUSSION

In this study, we proposed an approach of cooperating the BDS, GPS, GLONASS and SM records for real-time deformation monitoring, which was validated by the experimental data. In this approach, the GNSS data were processed with the RTK technology to retrieve the GNSS displacement, while the SM data was calibrated to get the raw acceleration; a Kalman filter was used to combine the GNSS displacement and the SM acceleration to obtain the integrated displacement, velocity and acceleration. The validation results show that the advantages of

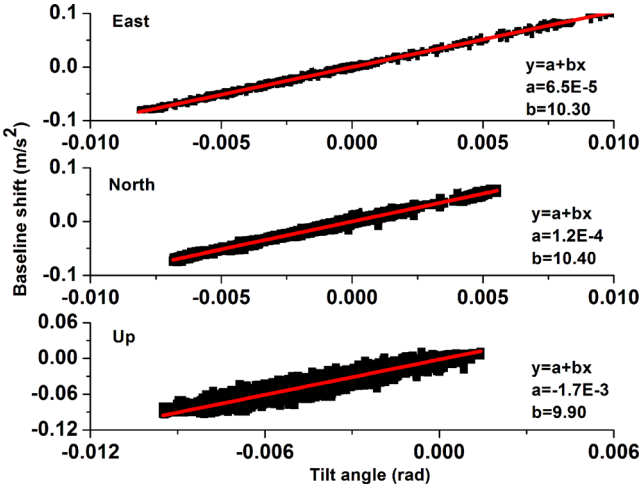

Figure 10. The relationship between the estimated baseline shift error and the ground tilting (the red line shows the linear fitting).

each sensor are completely complementary: for the SM, the baseline shifts are estimated and corrected, and the high-precision velocity and displacement are recovered; and for the GNSS, the noise are reduced by using the SM's high-resolution acceleration, thus the high-precision and broad-band deformation information can be obtained in real time. The relationships between the baseline shift and the ground tilting are also analysed. Their directly strong proportional relationships infer that estimating the baseline shift error as an unknown parameter is more objective than applying the empirical correction approach.

Nowadays, the deformation monitoring is commonly carried out in our daily life, such as the high building, dam, bridge, landslide and others. Up to now, using only one kind of sensors shows its limitation, and the cooperation of different sensors can complement the advantages of each other and provide more robust information. In this study, we investigated a data solution approach to combine the BDS, GPS, GLONASS and SM records, which is operated on the microcomputer by utilizing two separate instruments. The development of an integrated hardware and software system is of more interest and will be studied in the future work.

Furthermore, the approach needs to be tested in the demonstration project to better improve the reliability and continuity, especially for those conditions where the deformation area is relatively large and/or the observation environment is of poor conditions. In addition, for the earthquake monitoring, the movements may spread up to hundreds and/or thousands kilometres, where the RTK technology cannot be performed. Thus in future, the PPP technique may become another more competitive tool than the RTK in terms of the integration of GNSS and SM.

ACKNOWLEDGEMENTS

The work was partly supported by the program of National Key Research and Development Plan of China (grant no. 2016YFB0501804), National Natural Science Foundation of China (grant nos 41504006 and 41674034) and Chinese Academy of Sciences (CAS) programs of 'Pioneer Hundred Talents', and 'The Frontier Science Research Project' (grant no. QYZDB-SSW-DQC028).

REFERENCES

Blewitt, G., 1989. Carrier phase ambiguity resolution for the Global Positioning System applied to geodetic baselines up to 2000 km, *J. geophys. Res.,* **94,** 10 187–10 203.

Bock, Y., Melgar, D. & Crowell, B.W., 2011. Real-time strong-motion broadband displacements from collocated GPS and accelerometers, *Bull. seism. Soc. Am.,* **101,** 2904–2925.

Boore, D.M., 2001. Effect of baseline corrections on displacement and response spectra for several recordings of the 1999 Chi-Chi, Taiwan, earthquake, *Bull. seism. Soc. Am.,* **91,** 1199–1211.

Cai, C. & Gao, Y., 2007. Precise point positioning using combined GPS and GLONASS observations, *J. Global Position. Syst*., **6**(1), 13–22.

Chen, Q.J., Niu, X.J., Zhang, Q. & Cheng, Y., 2015. Railway track irregularity measuring by GNSS/INS integration, *J. Inst. Navig.,* **62**(1), 83–93.

Colosimo, G., Crespi, M. & Mazzoni, A., 2011. Real-time GPS seismology with a stand-alone receiver: a preliminary feasibility demonstration, *J. geophys. Res.,* **116,** B11302, doi:10.1029/2010JB007941.

Dong, D.N. & Bock, Y., 1989. Global Positioning System network analysis with phase ambiguity resolution applied to crustal deformation studies in California, *J. geophys. Res*., **94,** 3949–3966.

Elósegui, P., Davis, J.L., Oberlander, D., Baena, R. & Ekström, G., 2006. Accuracy of high-rate GPS for seismology, *Geophys. Res. Lett.,* **33,** L11308, doi:10.1029/2006GL026065.

Emore, G.L., Haase, J.S., Choi, K., Larson, K.M. & Yamagiwa, A., 2007. Recovering seismic displacements through combined use of 1-Hz GPS and strong-motion accelerometers, *Bull. seism. Soc. Am.,* **97,** 357–378.

Fleming, K. *et al.*, 2009.The Self-Organising Seismic Early Warning Information System (SOSEWIN), *Seismol. Res. Lett.,* **80,** 755–771.

Ge, M., Gendt, G., Rothacher, M., Shi, C. & Liu, J., 2008. Resolution of GPS carrier-phase ambiguities in precise point positioning (PPP) with daily observations, *J. Geod.,* **82**(7), 389–399.

Geng, J. & Shi, C., 2017. Rapid initialization of real-time PPP by resolving undifferenced GPS and GLONASS ambiguities simultaneously, *J. Geod.,* **91**(4), 361–374.

Geng, J., Meng, X., Dodson, A., Ge, M. & Teferle, F., 2010. Rapid reconvergences to ambiguity-fixed solutions in precise point positioning, *J. Geod.,* **84**(12), 705–714.

Geng, J., Teferle, F.N., Meng, X. & Dodson, A.H., 2011. Towards PPP-RTK: ambiguity resolution in real-time precise point positioning, *Adv. Space Res.,* **47**(10), 1664–1673.

Geng, J., Bock, Y., Melgar, D., Crowell, B.W. & Haase, S., 2013a. A new seismogeodetic approach applied to GPS and accelerometer observations of the 2012 Brawley seismic swarm: implications for earthquake early warning, *Geochem. Geophys. Geosyst.,* **14**(7), 2124–2142.

Geng, J., Melgar, D., Bock, Y., Pantoli, E. & Restrepo, J., 2013b. Recovering coseismic point ground tilts from collocated high-rate GPS and accelerometers, *Geophys. Res. Lett.,* **40,** 5095–5100.

Genrich, J.F. & Bock, Y., 2006. Instantaneous geodetic positioning with 10–50 Hz GPS measurements: noise characteristics and implications for monitoring networks, *J. geophys. Res.,* **111,** B03403, doi:10.1029/2005JB003617.

Iwan, W., Moser, M. & Peng, C., 1985. Some observations on strong-motion earthquake measurement using a digital accelerograph, *Bull. seism. Soc. Am.,* **75,** 1225–1246.

Javelaud, E.H., Ohmachi, T. & Inoue, S., 2011. A quantitative approach for estimating coseismic displacements in the near field from strong-motion accelerographs, *Bull. seism. Soc. Am.,* **101,** 1182–1198.

Jokinen, A., Feng, S. & Milner, C., 2011. Precise Point Positioning and Integrity monitoring with GPS and GLONASS, in *European Navigation Conference 2011*, London, U.K.

Li, X., Zhang, X. & Ge, M., 2011. Regional reference network augmented precise point positioning for instantaneous ambiguity resolution, *J. Geod.,* **85**(3), 151–158.

Li, X., Ge, M., Zhang, Y., Wang, R., Klotz, J. & Wicket, J., 2013a. High-rate coseismic displacements from tightly-integrated processing of raw GPS and accelerometer data, *Geophys. J. Int.,* **195,** 612–624.

Li, X., Ge, M., Guo, B., Wickert, J. & Schuh, H., 2013b. Temporal point positioning approach for real-time GPS seismology using a single receiver, *Geophys. Res. Lett.,* **40,** 5677–5682.

Li, X., Ge, M., Dai, X., Ren, X., Fritsche, M., Wickert, J. & Schuh, H., 2015a. Accuracy and reliability of multi-GNSS real-time precise positioning: GPS, GLONASS, BeiDou, and Galileo, *J. Geod.,* **89**(6), 607–635.

Li, X., Zus, F., Lu, C., Dick, G., Ning, T., Ge, M., Wickert, J. & Schuh, H., 2015b. Retrieving of atmospheric parameters from multi-GNSS in real-time: validation with water vapor radiometer and numerical weather model, *J. geophys. Res.,* **120**(14), 7189–7204.

Li, M., Li, W.W., Fang, R.X., Shi, C. & Zhao, Q.L., 2015c. Real-time high-precision earthquake monitoring using single-frequency GPS receivers, *GPS Solut.,* **19**(1), 27–35.

Liu, Y., Ye, S., Song, W., Lou, Y. & Chen, D., 2017. Integrating GPS and BDS to shorten the initialization time for ambiguity-fixed PPP, *GPS Solut.,* **21**(2), 333–343.

Tu, R., 2014. Fast determination of displacement by PPP velocity estimation, *Geophys. J. Int.,* **196**(3), 1397–1401.

Tu, R., Wang, R., Ge, M., Walter, T.R., Ramatschi, M., Milkereit, C., Bindi, D. & Dahm, T., 2013. Cost effective monitoring of ground motion related to earthquakes, landslides or volcanic activities by joint use of a single-frequency GPS and a MEMS accelerometer, *Geophys. Res. Lett.,* **40**(15), 3825–3829.

Tu, R., Ge, M., Wang, R. & Walter, T.R., 2014. A new algorithm for tight integration of real-time GPS and strong-motion records, demonstrated on simulated, experimental, and real seismic data, *J. Seismol.,* **18**(1), 151–161.

Wang, R., Parolai, S., Ge, M., Jin, M.P., Walter, T.R. & Zschau, J., 2013. The 2011 Mw 9.0 Tohoku earthquake: comparison of GPS and strong-motion data, *Bull. seism. Soc. Am.,* **103**(2B),1336–1347.

Wang, R., Schurr, B., Milkereit, C., Shao, Z. & Jin, M., 2011. An improved automatic scheme for empirical baseline correction of digital strong-motion records, *Bull. seism. Soc. Am.,* **101,** 2029–2044.

Wu, Y. & Wu, C., 2007. Approximate recovery of coseismic deformation from Taiwan strong-motion records, *J. Seismol.,* **11,** 159–170.

Xu, P., Shi, C., Fang, R., Liu, J., Niu, X., Zhang, Q. & Yanagidani, T., 2013. High-rate precise point positioning (PPP) to measure seismic wave motions: an experimental comparison of GPS PPP with inertial measurement units, *J. Geod.,* **87**(4), 361–372.

Yanase, T., Tanaka, H., Ohashi, M., Kubo, Y. & Sugimoto, S., 2010. Long baseline relative positioning with estimating ionosphere and troposphere gradients, in *23rd International Technical Meeting of the Satellite Division of the Institute of Navigation*, OR, September 21–24, 2010.

Zumberge, J.F., Heflin, M.B., Jefferson, D.C. & Watkins, M., 1997. Precise Point Positioning for the efficient and robust analysis of GPS data from large networks, *J. geophys. Res.,* **102,** 5005–5017.